Application of Transpiration Cooling for Hot Structures

M. Kuhn and H. Hald

Deutsches Zentrum für Luft- und Raumfahrt e.V.
Institut für Bauweisen- und Konstruktionsforschung
Pfaffenwaldring 38-40, D-70569 Stuttgart, Germany
markus.kuhn@dlr.de

Summary

Specific parts of re-entry vehicles are exposed to severe conditions. Thereby, the material's capabilities can be exceeded by far and advanced cooling methods become necessary. Within the scope of this work, transpiration cooling was investigated in arc jet heated plasma flows by means of flat plate models. Screening tests pointed out, that transpiration cooling at the conditions tested is working well. Extensive testing at more severe conditions was done using three porous sample materials: Standard C/C with coolant flows parallel and perpendicular to the material's fibre layers and highly porous C/C. Coolant gases used were air, argon, helium and nitrogen. Minimal optimal coolant mass flows of 0.5 g/s Ar, 0.2 g/s He and 0.4 g/s N_2 were determined resulting in sample under surface temperature reductions of 50-60%. Altogether, sample under surface temperature reductions of 64% for He, 65% for Ar, 67% for air and 70% for N_2 were detected. These test series verified that transpiration cooling can be applied successfully for hot structures at application relevant re-entry conditions.

1 Introduction

1.1 Background

For highly demanded parts of re-entry vehicles, high temperature usable materials like ceramic matrix composites (CMC's) are being used. Such parts are in particular thermal protection system elements and hot structures like leading edges, flaps or components of propulsion systems. In most cases, the cooling of such hot structures relies on radiation cooling. However, in some situations the material's capabilities can be exceeded, for instance by higher-energetic (interplanetary) re-entry conditions, smaller structure nose radii or higher ballistic coefficients. Therefore, e.g. ablative or advanced cooling techniques like active cooling systems become necessary. Thereby, reusability is a great advantage of active cooling systems in contrast to ablative ones.

1.2 Motivation

Active cooling systems usually consist of internally, convective cooled structures like heat pipes. Additionally, it is possible to perform external active cooling systems; such systems could be for example transpired surfaces, which have not been applied successfully to reusable spacecraft yet. Basically, the principle of transpiration

A. Gülhan (Ed.): RESPACE – Key Tech. for Reusable Space Sys., NNFM 98, pp. 82–103, 2008.
springerlink.com

cooling consists of two heat mechanisms (see Fig. 1): Firstly, the porous structure is being cooled by convection of the coolant flow penetrating the porous media. Secondly, a thermal blocking coolant layer is built on the outer, hot surface of the porous structure, which tremendously reduces heat transfer to the outer surface.

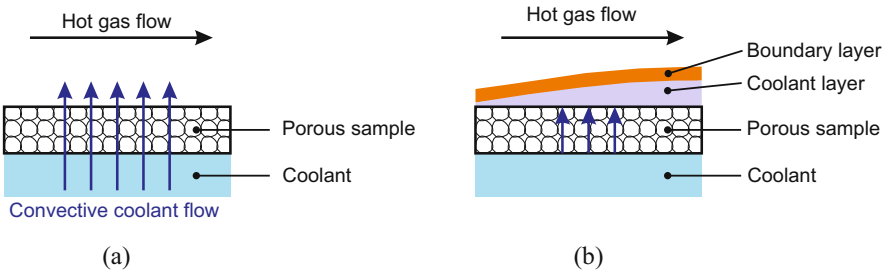

Fig. 1. Transpiration cooling mechanisms: (a) convective, (b) coolant layer

Already during the 50 s to 70 s, early studies of film, effusion and transpiration cooling have been done. Thereby, the main focus was laid on the cooling of gas turbine blades, rocket combustion chambers and hot structures like e.g. nose tip regions of intercontinental ballistic missiles. There are a lot of analytical and experimental approaches out of this time period, e.g. [9, 12, 13, 15, 16], but none of them contained experimental tests at low pressure supersonic plasma flow conditions. Although first considerations of such cooling methods for spacecraft existed during this time, no further investigations were made due to the lack of appropriate porous materials. In the 90's, those cooling techniques became interesting again and some detailed simulations were done, e.g. [1, 3, 8, 14, 19]. Since a couple of years, DLR is successfully working on transpiration-cooled rocket engines [2, 11, 18], which are fabricated out of porous CMC's. These materials are qualified candidates for transpiration cooling as they can be produced within a huge variety of open porosity and hence different permeability characteristics. Additionally, they exhibit excellent mechanical and thermal properties. Contrary to metal foams used until the 70s, CMC's do not fail if local hot spots occur. Metal foam structures tend to melt in the presence of local hot spots, which results in a whole structure failure. For more detailed information of DLR manufactured carbon- and oxide-based ceramics please refer to [6, 7, 17].

1.3 Proposed Aims

As there is a lack of experimental data for transpiration cooled CMC's in hypersonic plasma flows, the key aspects are laid on the experimental verification of such a cooling technique. The aim of this investigation is to estimate the effect of transpired surfaces for different gaseous coolant types and coolant mass flows as well as different sample materials. Those samples should be exposed to re-entry conditions in arc jet heated, hypersonic flows.

Therefore, already existing model holders should be modified and used for screening test series in facilities L2K and L3K [4, 5] in order to estimate the cooling influence of

different coolants for different sample materials. Based on the experiences made there, a more detailed, final test series in the L3K facility should be performed. More detailed information of the testing facilities can be obtained in Chapter 7.

2 Design of Experimental Setup

2.1 Screening Test Series in L2K / L3K

Figures 2a and b show a basic setup of the models used in L2K and L3K. It is possible to incline the models at different angles of attack α in order to achieve variable heat loads. They consist of a water-cooled copper nose section, which is rigidly coupled with a water-cooled ground plate. Directly onto this plate, the coolant supply assembly is mounted, where different fed in coolant gases pass through a circular porous sample. Before and after the supply assembly, KAPYROK insulation material was placed, which consists of 91% aluminium oxide Al_2O_3 and 9% silicon oxide SiO_2. Thereby, heat transfer between the supply assembly and surrounding parts, particularly the water-cooled nose section should be avoided.

Figure 3 shows a schematic of the coolant supply assembly, forming the central part of the model. Basically, for both models used, the components are almost identical, though there are minor differences at some parts. A two-piece frame structure (2) made of stainless steel for L2K tests and of C/C-SiC for L3K tests, respectively, builds the skeletal structure for the assembly. Inside, a C/C-SiC cover plate (3) is attached, which was superimposed with a 100 µm thick, multilayered CVD-SiC coating for the L2K model to improve oxidation resistance. For the L3K model, no coating was applied. This cover plate holds a circular porous CMC sample (4), which is bonded with its conical section onto the conical counterpart of a reservoir tube made of C/C-SiC (5). The hereby used bond (*Polytec* 904) is based on ZrO_2 capable of resisting temperatures up to 2200°C. The reservoir tube is glued on an aluminium ring by means of an epoxy resin, which enables O-ring sealing to the supply rig (6) made of stainless steel. Using this rig, the coolant gas supply as well as two thermo-couples and a pressure sensor are being fixed. To support the bond between sample and reservoir tube, a spring mechanism is integrated to impose

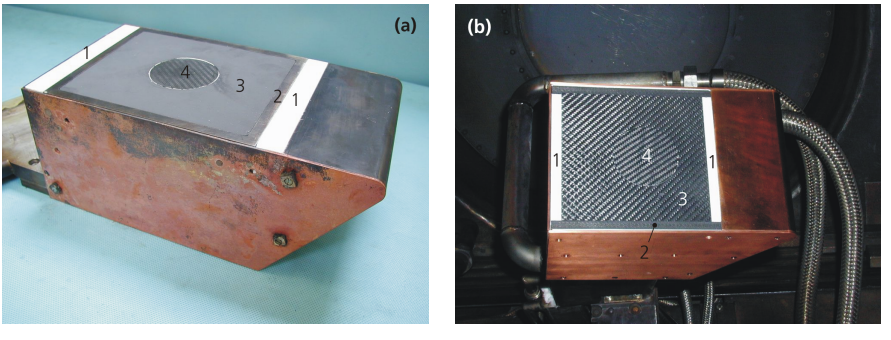

Fig. 2. Screening test models: (a) L2K model, (b) L3K model; 1 = KAPYROK insulation, 2 = frame structure, 3 = cover plate, 4 = porous sample

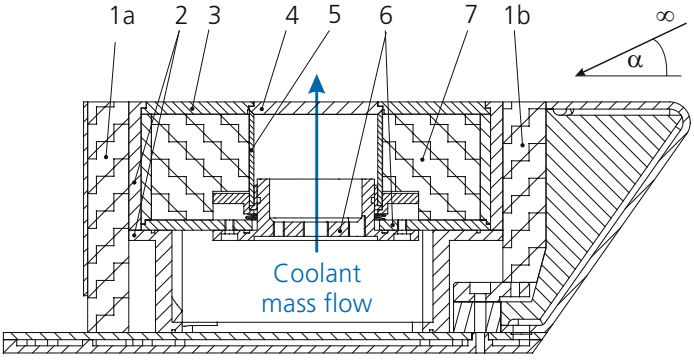

Fig. 3. Schematic of supply assembly for screening tests; 1a+b = KAYPROK insulation, 2 = frame structure, 3 = cover plate, 4 = porous sample, 5 = reservoir tube, 6 = supply rig, 7 = inner KAPYROK insulation

pressure upon the reservoir tube (5). Additionally, inside the setup KAPYROK material (7) is inserted in order to insulate the coolant reservoir against the surrounding parts.

At the beginning, first screening tests were carried out at L2K to check the model setup and to estimate appropriate cooling mass flow rates. Based on these experiences, a similar setup was made for L3K facility, which enables higher heat loads to the transpired samples. Due to different model holders in L2K and L3K, the geometric dimensions of the entire L2K model were 295 x 156 x 122 mm, whereas the L3K model was 73 mm shorter in length. Additionally, the centre of the CMC sample was 182 mm downstream of the stagnation point for L2K tests and 135 mm for L3K tests, respectively.

As can be seen in Fig. 4, inside the setup two thermocouples have been installed: The first one was bonded into a very small gap at the under side of the sample and measures the under surface temperature of the sample downstream. The other one measures the coolant gas temperature in the reservoir. Additionally, a pressure sensor made by *Kulite* records coolant reservoir pressures up to 3.4 bars. From outside, pyrometry has been used upstream of the sample, onto the sample (only L3K) at the position where thermocouple 1 is and shortly after the sample downstream (only L3K). Also, IR-thermography has been applied to observe the cooling behaviour, mainly directly on the sample and in the wake of the transpired region.

For the screening test series, four CMC sample materials with different porosities have been used, which can be seen in Table 1. All carbon based CMC's were manufactured by the Institute of Structure and Design, DLR Stuttgart and had an exit diameter of 60 mm and thickness of 6 mm; aluminium oxide based WHIPOX, manufactured by Institute of Materials Research, DLR Cologne, was 3 mm thick. Due to the smaller material thickness of WHIPOX, an appropriate C/C-SiC retainer ring was fabricated, into which the WHIPOX samples were bonded. This reduced the sample exit diameter to 44 mm for WHIPOX samples. Open porosities varied from 13 to 41%. It is remarked, that for C/C-SiC, the coolant flow occurs parallel to the fibre layers, while for the other samples the coolant flow passes perpendicular through to the fibre layers via micro cracks (see Fig. 5).

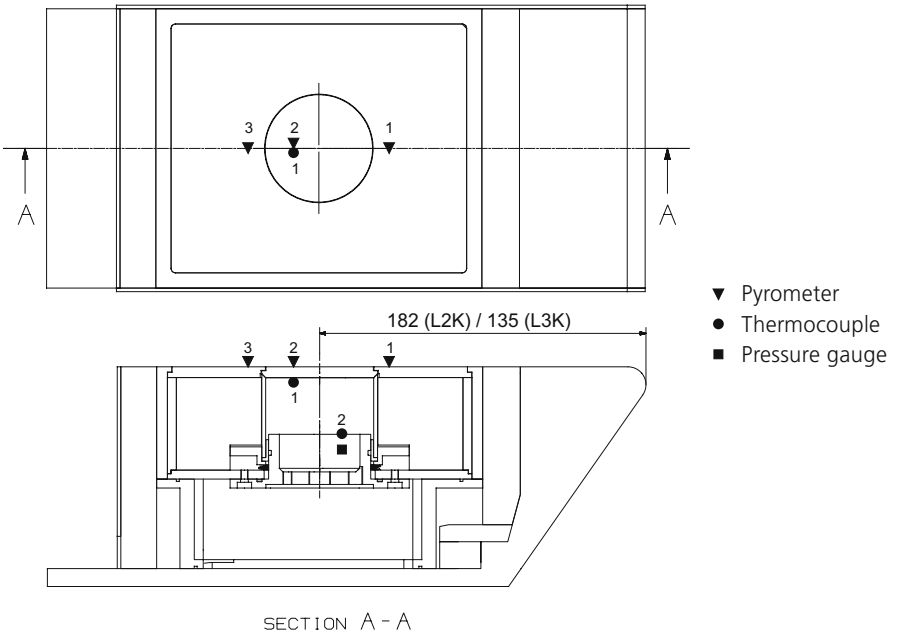

Fig. 4. Position of sensors for screening tests

Table 1. Sample materials for screening tests

Material	Coolant flow	*e'* [%]	*d* [mm]	Ø [mm]	*A* [m²]	Used in L2K	Used in L3K
C/C highly porous	⊥	41	6	60	$2{,}827 \cdot 10^{-3}$	×	×
C/C standard	⊥	13	6	60	$2{,}827 \cdot 10^{-3}$	×	×
C/C-SiC	∥	15	6	60	$2{,}827 \cdot 10^{-3}$	×	
WHIPOX	⊥	33	3	44	$1{,}521 \cdot 10^{-3}$	×	×

e' open porosity, *d* thickness, Ø exit diameter, *A* exit area.

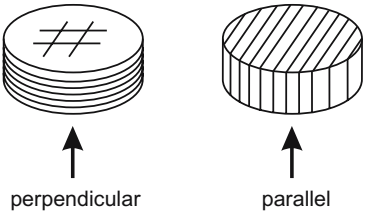

Fig. 5. Coolant flow direction relating to sample fibre layers

2.2 Main Test Series in L3K

Many experiences have been made at the screening test series; especially sealing problems have been detected as major challenges. At high heat loads for instance,

different thermal expansion characteristics of the reservoir tube and the glued on aluminium ring caused the reservoir tube to break. Supplementary, rapid increases of heat fluxes onto the sample – and hence transferred heat to the bonded joint between reservoir tube and sample – caused the ceramic bond to break due to insufficient resistance to thermal shocks. From this follows that a leakage of the coolant reservoir makes further testing useless.

Therefore, the setup has been modified at the appropriate parts. Figures 6a and b show the model setup for the main test series conducted in L3K. Just like at the previous models, it is possible to incline the model at different angles of attack in order to achieve variable heat loads. Regarding the setup, the model bases upon a water-cooled copper nose section rigidly coupled with a water-cooled ground plate. Onto this plate, the coolant supply assembly is mounted, where different fed in coolant gases pass through a rectangular porous sample embedded in a cover frame. Around the supply assembly, KAPYROK insulation material was inserted in order to avoid heat transfer between the outer, hot parts and the inner, water-cooled parts.

Figure 7 shows an exploded view of the coolant supply assembly for the main test model. The whole assembly is fixed to a substructure made of copper and stainless steel (8), which is installed onto the ground plate of the model holder itself. Directly onto this substructure, the coolant reservoir (7) is being placed, whereas at the reservoir sidewalls the coolant supply and sensors are attached. On top of the reservoir, the porous sample (6) and a graphite seal (5) are placed. In the following, a metallic sealing unit (4) made of *Plansee* PM 2000 material is attached – this part can be screwed together with the substructure which effects, that the porous sample can be sealed against the coolant reservoir. To avoid heating of the metallic sealing unit, insulation (3) made of aluminium oxide fleece was positioned between the sealing unit (4) and cover frame (2) made of C/C-SiC. Around the cover frame and porous probe a C/C-SiC cover plate (1) is attached, which was superimposed with a 100 µm thick, multilayered CVD-SiC coating to improve oxidation resistance.

For this model, another holder has been used which effected in smaller height and greater width; geometric dimensions of the model were 285.5 x 194 x 60 mm. Thereby, the centre of the samples was positioned 107.1 mm downstream of the stagnation point and 40 mm distant to the model centreline. Contrary to previous models, the samples used here were rectangular with exit dimensions of 61 x 61 mm and they were placed at

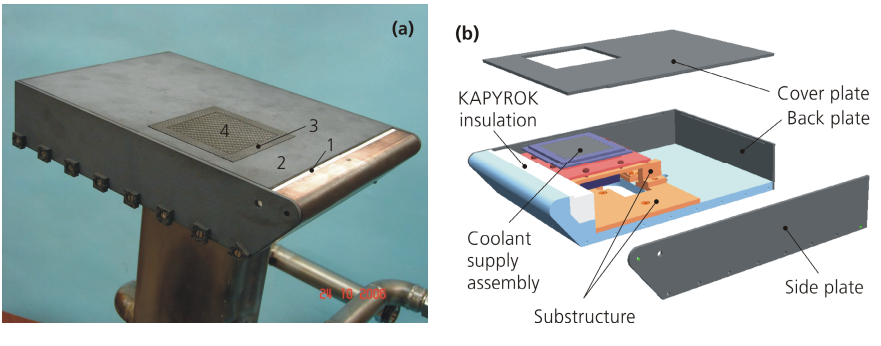

Fig. 6. (a) Main test model and its (b) exploded view (without inner insulation), 1 = KAPYROK insulation, 2 = cover plate, 3 = cover frame, 4 = porous sample

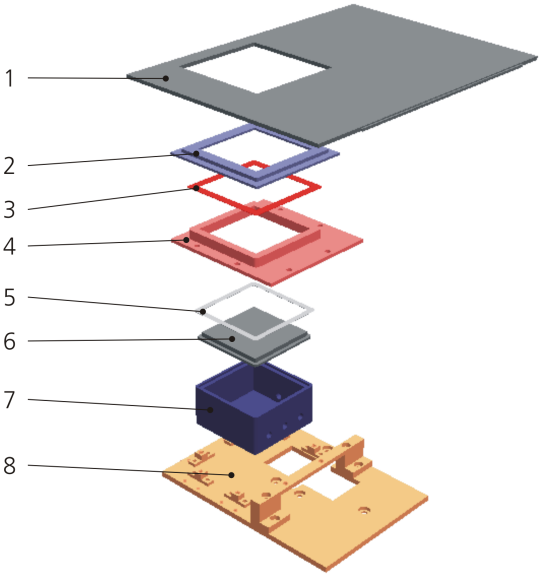

Fig. 7. Schematic of supply assembly for main tests; 1 = cover plate, 2 = cover frame, 3 = insulation, 4 = sealing unit, 5 = graphite seal, 6 = porous sample, 7 = coolant reservoir, 8 = substructure

one model half only, as can be seen in Fig. 8. This results in a cooled and uncooled side, which makes direct estimations of the cooling effects possible.

Furthermore, additional sensors have been installed as can be seen in Fig. 8. Besides the pressure measurement in the coolant reservoir, it is possible to measure coolant gas temperature and sample under side temperature by means of a thermocouple bonded into a small gap in the sample. At the same position of the sample on top, a pyrometer spot was placed, which records the sample surface temperature. To compare the cooling effect, two pyrometers were placed on the uncooled side (with same distance to the stagnation point as the sample pyrometer spot) and two more pyrometers upstream of the sample. Twelve additional thermocouples were attached in different heights inside the setup in order to estimate the cooling effect onto the internal structure. Furthermore, IR-thermography has been applied to observe the cooling behaviour.

For the main test series, three CMC sample materials with different porosities have been tested, which can be seen in Table 2. Only carbon based CMC's manufactured by the Institute of Structure and Design, DLR Stuttgart with exit dimensions of 61 x 61 mm and thickness of 6 mm have been used; aluminium oxide based WHIPOX [17] and OXIPOL [7] are considered to be tested in near future. Open porosities varied from 16 to 44%. Extensive testing has been made with standard C/C material, which can be produced very well regarding reproducibility and quality. Additionally, stratified C/C based on standard C/C material has been used. It is marked by C/C standard $\|$, because coolant flow occurs parallel to the fibre layers here. The last material tested was highly porous C/C.

Table 2. Sample materials for main tests

Sample material	Coolant flow	*e'* [%]	*d* [mm]	*x·y* [mm]	*A* [m²]
C/C standard ⊥	⊥	17-18	6	61·61	$3{,}721 \cdot 10^{-3}$
C/C standard ‖	‖	16	6	61·61	$3{,}721 \cdot 10^{-3}$
C/C highly porous	⊥	44	6	61·61	$3{,}721 \cdot 10^{-3}$

e' open porosity, *d* thickness, *x·y* exit dimensions, *A* exit area.

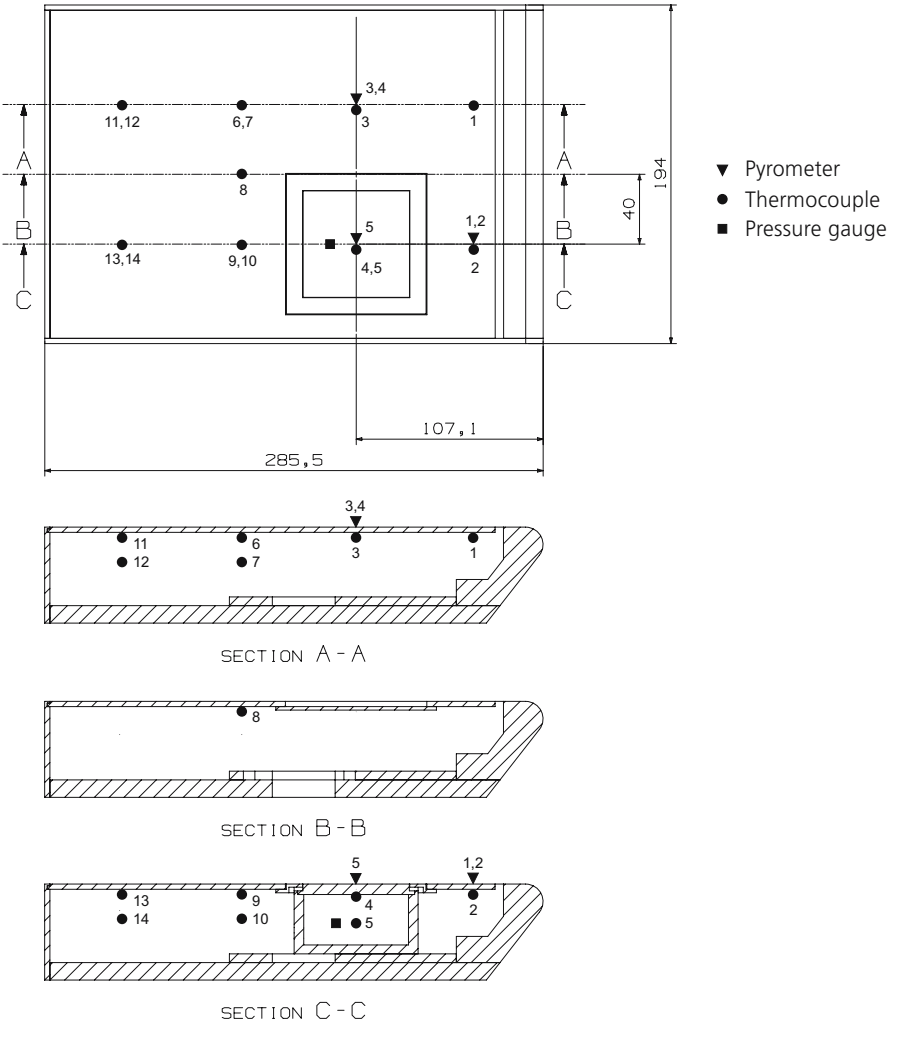

Fig. 8. Position of sensors for main tests

3 Experimental Results

A detailed description of the experimental facilities can be seen in Chapter 7.

3.1 Screening Tests

At the beginning, first tests were conducted at relatively moderate enthalpies at L2K facility. Afterwards, a second test series was carried out at L3K facility at higher enthalpies and hence higher surface temperatures. The more interested reader is referred to [10]. Flow conditions for both test series are shown in Table 3.

It was considered to compare different coolant gases based on equal volume flows. At operation, the coolant mass flows were adjusted proportional to the coolant gases densities at ambient conditions. Hence, e.g. a mass flow rate of 1.00 g/s N_2 would equal 0.14 g/s He or 1.43 g/s Ar.

Table 3. Flow conditions of screening tests

	L2K	L3K FC-II
Reservoir pressure [hPa]	1000	4550
Reservoir temperature [K]	4220	5400
Total enthalpy [MJ/kg]	8.4	11.0
Mass flow [g/s]	36	142
Nozzle exit diameter [mm]	200	300
Model position downstream [mm]	250	300
Free stream Mach number [-]	7.0	7.6
Free stream static pressure [Pa]	47	50
Free stream static temperature [K]	378	491
Angle of attack [°]	20	30
Free stream velocity [m/s]	2996	3730
Mass fraction N_2	0.739	0.757
Mass fraction O_2	0.046	0.012
Mass fraction NO	0.045	0.018
Mass fraction N	$< 10^{-6}$	$< 10^{-6}$
Mass fraction O	0.170	0.213

Screening tests L2K

Main goals of this attempt were to determine, which sample materials are suited for this kind of cooling. Additionally, different coolant gases should be used in order to determine efficiency of the gas itself and the required mass flows. All tests were performed by inserting the model without cooling gases switched on and thereby heating up the whole configuration. After reaching sample under surface temperatures of about 700 K, the coolant gases where switched on and increased stepwise. Coolant gases used for these tests were N_2, He, Ar and air at typical test times of about 400 s. Maximum coolant gas pressures recorded in the reservoir were about 3.0 bars for standard C/C, 1.1 bars for highly porous C/C, 1.6 bars for WHIPOX and 0.2 bars for C/C-SiC.

Figure 9 shows typical temperature traces of the cover plate (upstream of the sample), coolant gas and the sample under surface for a WHIPOX sample and

different nitrogen coolant mass flows. Due to short test times, no steady state conditions could be reached. Nevertheless, the temperature at the lower sample surface was assumed to be quasi-stationary at the end of each mass flow step. A further unfavourable effect is the rising of coolant gas temperature by time; this can be explained by the heating of the whole setup from top, which heats up the coolant gas as well. Hence, the reduction of sample under surface temperatures will not be that effective after several small coolant mass flow steps as if the final coolant mass flow would be switched on directly.

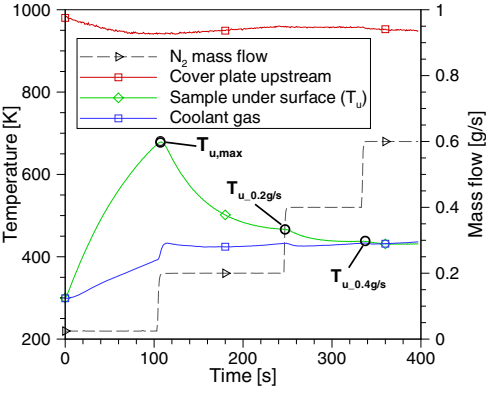

Fig. 9. Typical temperature traces at $\alpha = 20°$, coolant: N_2, sample: WHIPOX

To estimate the cooling efficiency, these quasi-stationary values were used. Usually, for film cooling comparability, the cooling efficiency η is defined by the ratio of Stanton numbers or heat fluxes for the cooled (index c) in relation to the uncooled case (index 0)

$$\eta(F) = 1 - \frac{St_c}{St_0} = 1 - \frac{\dot{q}_c}{\dot{q}_0} \tag{1}$$

This efficiency is dependent on the blowing ratio F, which is defined by the ratio of ρu for the coolant (index c) in relation to the flow conditions at the outer edge of the boundary layer (index e)

$$F = \frac{(\rho u)_c}{(\rho u)_e} \tag{2}$$

Determination of heat fluxes according to Eq. 1 for this kind of plasma flows is difficult to perform due to high temperature effects. This problem is well known and will have to be investigated more in future. Furthermore, the integration of a heat flux sensor into the porous sample would be unfavourable as it would disturb the coolant flow through the porous sample.

Additionally, a detached, curved shock wave forms at the nose part of the holder. Unfortunately, the flow conditions after the shock at the sample position is not

known. Also, the effective open pore area of the porous samples was not known, from which the coolant velocity u could be calculated by means of continuity. Hence, the blowing ratio F (Eq. 2) is not formed here and the coolant mass flow is used therefore. Instead of η, an alternative comparability number Z is defined, which describes the temperature decrease at the sample under surface in comparison to the maximum occurring temperature

$$Z = \frac{T_{u,\max} - T_{u,\dot{m}}}{T_{u,\max}} \cdot 100\% \,. \tag{3}$$

Hereby, $T_{u,\dot{m}}$ are the temperatures at the sample under surface after each coolant mass flow step (see Fig. 9). $T_{u,max}$ is the maximum occurring temperature at the end of the heating phase and acts as reference temperature, which is between 450 and 760 K.

Figures 10a-d show the comparability numbers Z for all samples and coolant gases tested. It can be seen, that there is a different trend for each coolant gas at same gas

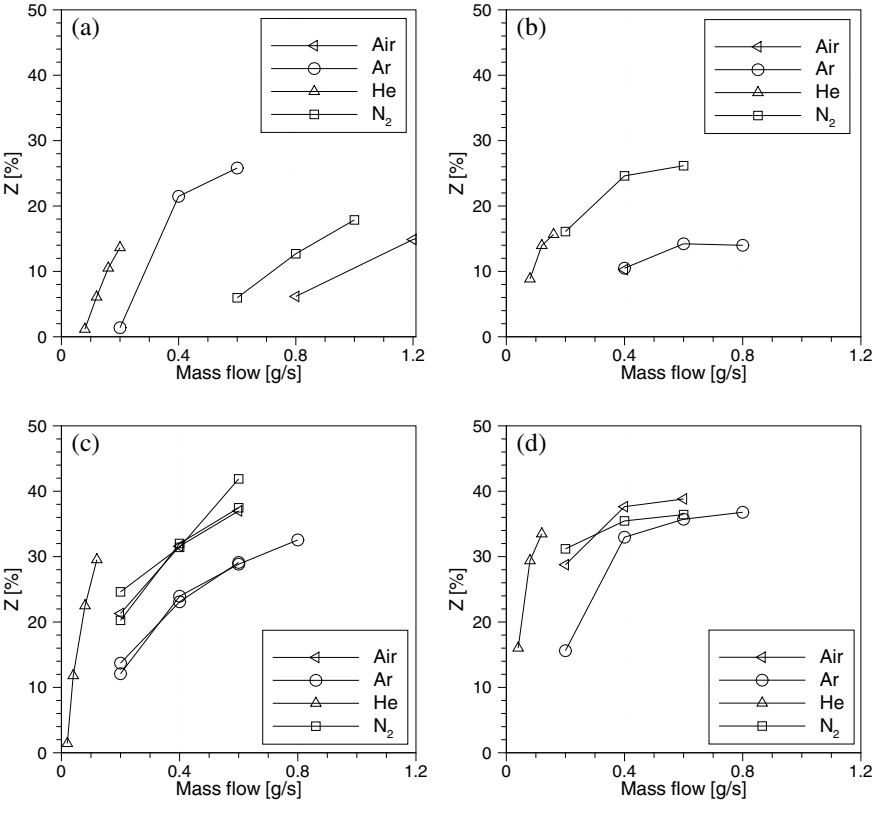

Fig. 10. Comparability number Z at $\alpha = 20°$ for (a) C/C standard, (b) C/C highly porous, (c) C/C-SiC, (d) WHIPOX

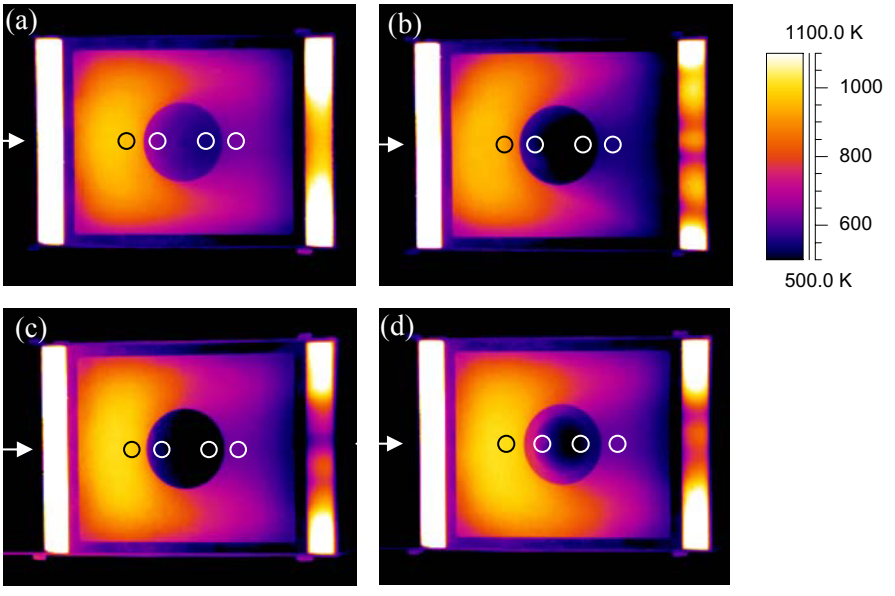

Fig. 11. IR-thermography for nitrogen mass flows of 0.4 g/s at $\alpha = 20°$; (a) C/C standard, (b) C/C highly porous, (c) C/C-SiC, (d) WHIPOX

volume flows. N_2 seems to be the most efficient coolant of all followed by air and Ar. Contrary to all other coolants, He turned out to be less effective. This leads to the assumption that coolant properties like heat conductivity or capacity have to be considered more detailed in future. There is only one exception that exists for standard C/C (Fig. 10a). Ar seems to be more effective as N_2 or air.

Taking a closer look on the different porous sample materials, it can be concluded, that for highly permeable samples like C/C-SiC and WHIPOX, the efficiency is increased significantly. But is has to be remarked, that for C/C-SiC, the fibre layers are in coolant flow direction and WHIPOX had a thickness of only 3 mm. One explanation could be the holding time of the coolants while passing the porous sample. This time will be less as for highly porous or standard C/C, hence the convective heat transfer in the structure will be lower, but the thermal blocking effect in the boundary layer higher as the coolant enters the boundary layer slightly cooler.

In total, maximum temperature reductions Z of 34% for helium, 36% for argon, 38% for air and 42% for nitrogen are achieved.

For the following investigations, all different sample materials are compared with N_2 cooling. In order to see, how homogeneous the coolant blowing is, IR-thermography has been applied, which can be seen in Fig. 11 for nitrogen mass flows of 0.4 g/s.

Hereby, the flow direction was from the left. It can clearly be seen, that the cooling gas significantly reduces the sample temperatures in contrast to the cover plate upstream. It seems that the temperature decrease is greatest for highly porous C/C. However, temperature irregularities can be seen on top of the sample. This indicates, that the coolant gas escapes inhomogeneous, which can also be seen in three darker stripes at the KAPYROK insulation material downstream. These KAPYROK bars are white in colour due to different surface emissivity characteristics.

For standard C/C, blowing is very uniform; sample surfaces seem to be nearly isothermal and the wake region at the position of the KAPYROK blocks looks very homogeneous showing no darker stripes.

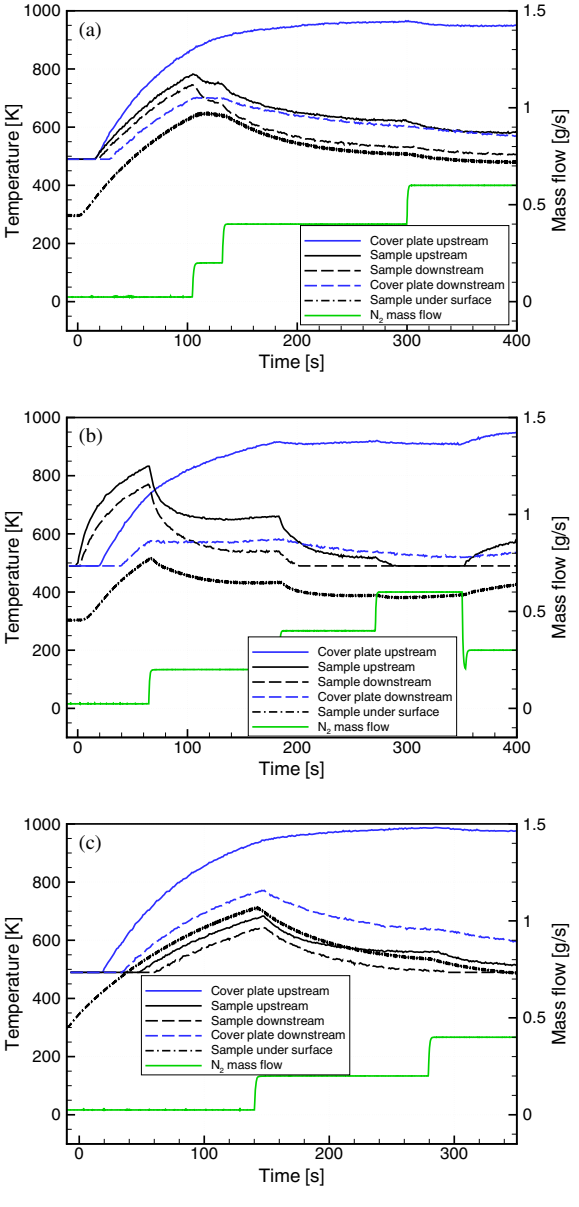

Fig. 12a-c. IR-thermography spots for coolant N_2 at $\alpha = 20°$; (a) C/C standard, (b) C/C highly porous, (c) C/C-SiC

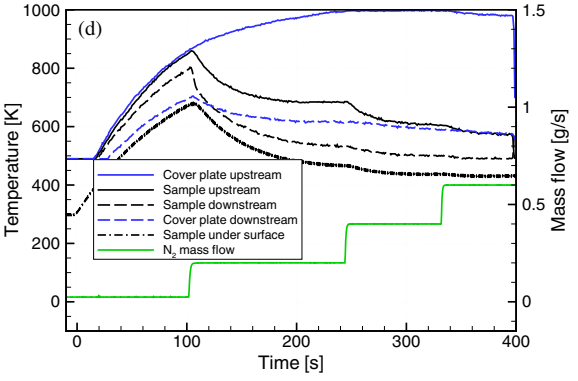

Fig. 12d. IR-thermography spots for coolant N_2 at $\alpha = 20°$; (d) WHIPOX

C/C-SiC and WHIPOX appear to have a more homogeneous blowing at the sample surfaces, though there are minor inhomogeneities visible.

It is to remark, that no significant flow field disturbances can be seen herby.

Figures 12a-d show some temperature line plots for selected spots on the middle axis for each material and N_2 coolant mass flows. These spots accord to the indicated circled spots in Figs. 11a-d. It can be seen, that the temperatures decrease over the length of the samples. Also to be noticed is the temperature decrease of the embedding C/C-SiC cover plate up- and downstream – whereby the cooling effect of the transpired samples even influences the temperatures of the cover plate upstream.

For C/C-SiC material, the sample under surface temperature seems to be higher than for the other sample materials. Possibly, due to high permeability of this material, hot gas is entering into the reservoir through the porous sample during the heating phase and so heating up the sample. Secondary, slightly uncertainties in sample emissivity characteristics and absorptance of the optical windows could explain this effect.

Screening tests L3K

The second screening test series in L3K should verify the experiences made in L2K at application relevant conditions and hence higher surface temperatures. This was mainly achieved by increasing the total enthalpy of the free stream, the static pressure at the model position and the angle of attack. Table 3 shows the flow condition "L3K FC-II" used hereby. Coolant gases used for L3K experiments were N_2 and He at typical test times of 180-220 s.

Again, the model was inserted without cooling gases switched on and thereby heating up the whole configuration. After reaching sample under surface temperatures of about 800-1000 K, the coolant gases where switched on in one step to coolant mass flows of 1.0 g/s for N_2 and 0.2 g/s for He. Sample materials tested were standard C/C, highly porous C/C as well as WHIPOX. Just like at L2K screening tests, N_2 turned out to be more effective than He [10].

Due to the higher surface temperatures, the internal supply assembly was heated up faster. This caused the coolant reservoir and hence coolant gas temperature heating up very quickly, which resulted in shorter test times. However, significant sealing problems at the coolant gas reservoir occurred.

Higher heating loads effected that the reservoir liner broke and a leakage developed, as can be seen in Fig. 13. Due to different thermal expansion characteristics of the reservoir tube and the glued on aluminium ring a crack in longitudinal direction was observed. The brownish colouration inside the C/C-SiC liner arises from silicone sealing material, which was tried to apply in order to seal the material.

The second weak point of this setup was the bonded joint between reservoir tube and sample. The rapid surface temperature increase after insertion of the model caused the ceramic bond to break and build micro cracks due to insufficient resistance to thermal shocks.

The problems mentioned yielded in a stop of this test series. Though the measurement results obtained were not quite good, the know-how regarding sealing problems gained here was worth a lot for prospective model setups.

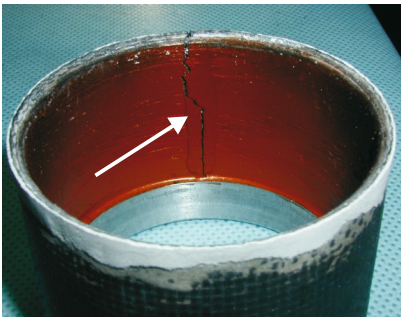

Fig. 13. Broken coolant reservoir at L3K screening tests

3.2 Main Tests L3K

Based on the experiences made at the two screening test series, a new model had been built. Critical parts like the coolant reservoir had been modified and fabricated out of C/C-SiC in two versions. One reservoir was made by means of castings, while the other one was fabricated out of thicker C/C-SiC plate material. Sealing of the reservoir was managed by a graphite seal. The modifications did work well, so that the more severe flow condition “L3K FC-III” was used at 20° and 30° angle of attack, which is detailed in Table 4. Coolant gases used for these tests were N_2, He, Ar and air at typical test times of about 180-300 s, which is characterised by greyish shaded boxes in the following diagrams. Also, several test runs have been performed to check repeatability, which was in very good agreement.

Again, it was considered to compare different coolant gases based on equal volume flows. In contrast to the screening tests, the model was inserted with cooling gases switched on; in addition, only a fixed coolant mass flow was adjusted.

Table 4. Flow condition of main tests

	L3K FC-III
Reservoir pressure [hPa]	4700
Reservoir temperature [K]	5650
Total enthalpy [MJ/kg]	11.6
Mass flow [g/s]	142
Nozzle exit diameter [mm]	300
Model position downstream [mm]	300
Free stream Mach number [-]	7.5
Free stream static pressure [Pa]	56
Free stream static temperature [K]	530
Angle of attack [°]	20 / 30
Free stream velocity [m/s]	3873
Mass fraction N_2	0.7620
Mass fraction O_2	0.0040
Mass fraction NO	0.0064
Mass fraction N	0.0001
Mass fraction O	0.2270

In comparison to the screening test samples, the exit area of the main test samples was increased by 32%. Based on the detected (screening tests) coolant mass flows required for satisfying cooling effects, the coolant mass flows were also increased by approximately 30% at the beginning. Thereby, it turned out that the increased mass flows were too high. This indicates that the sealing mechanism of the new model setup works much better than at the screening tests; the entire coolant gas passes through the sample now, whereas at the screening tests minor leakages existed. To detect the leakage flow in the coolant reservoir, an impermeable metallic sample had been installed and the reservoir was pressurized. The leakage flows determined by pressure loss were 3‰ for N_2 and 4‰ for He, which can be neglected.

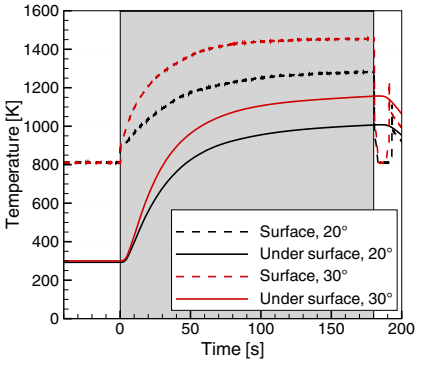

Fig. 14. Uncooled sample temperatures for C/C standard ⊥ at α = 20° / 30°

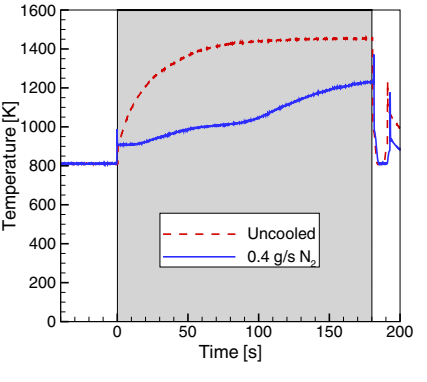

Fig. 15. Surface temperatures for standard C/C ⊥ at α = 30°; uncooled and for a nitrogen mass flow of 0.4 g/s

In the following, only details of the porous sample are discussed, which indicates the feasibility of transpiration cooled, hot structures. More detailed information of the other measurements can be seen in Chapter 7.

Although the model exhibits an uncooled half as reference, two tests without cooling have been performed at angles of attack α of 20° and 30°, which can be seen in Fig. 14. It shows the surface temperature measured by a pyrometer and the under surface temperature measured by a thermocouple for standard C/C ⊥ material. For α = 20°, temperatures of about 1300 K for the surface and 1000 K for the under surface were measured; for α = 30°, temperatures of about 1450 K for the surface and 1150 K for the under surface were measured.

With cooling, sample surface temperatures will be highly reduced, so that the temperatures are below the pyrometer's measurement range. Only for the uncooled cases at $\alpha = 20°$ and 30° and for a nitrogen mass flow of 0.4 g/s at $\alpha = 30°$, the surface temperatures where in the measurement range. Figure 15 shows the sample surface temperature measured by pyrometer for standard C/C ⊥ and the cases mentioned at $\alpha = 30°$. Here, it seems that a N_2 mass flow of 0.4 g/s is too low as the temperature doesn't reach stationary conditions and rises farther.

In order to compare the main tests with the screening tests, only under surface temperatures measured by thermocouple are discussed next. For C/C standard ⊥ samples, a series labelled by C/C-1 to C/C-3 originating from the same manufactured plate material was used thereby.

As can be seen in Fig. 16, for $\alpha = 20°$ no stationary conditions were achieved, but the influence of different mass flow rates can clearly be seen. While the reduction of a N_2 mass flow of 0.3 g/s seems to be too low, the effect of higher mass flows appears to be getting smaller. For $\alpha = 30°$ (see Fig. 16b), the temperatures are just slightly higher, although a higher angle of attack effects higher heat loads. Here, it seems that a N_2 mass flow of 0.4 g/s is too low as the temperature rises unproportional in contrast to higher mass flows. The cooling effect of N_2 and air is in good agreement for both angles of attack as expected due to similar physical properties.

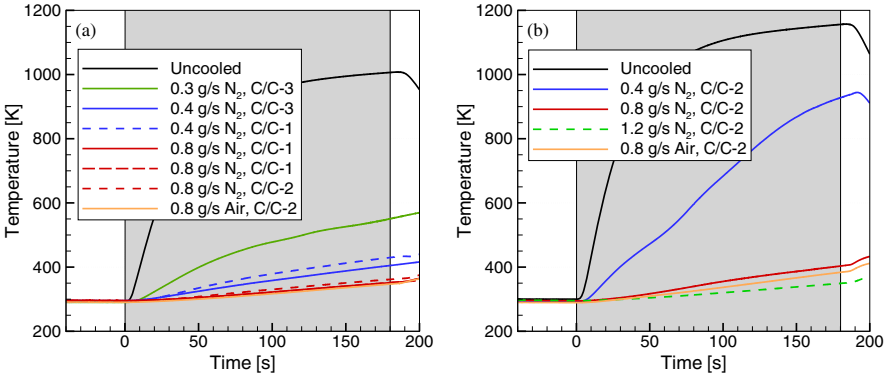

Fig. 16. Under surface temperatures for standard C/C ⊥ and coolants air and N_2, (a) α = 20° and (b) α = 30°

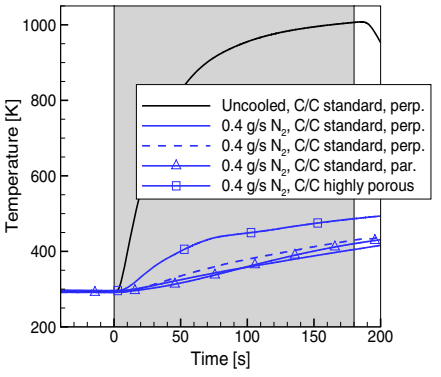

Fig. 17. Under surface temperatures for a nitrogen mass flow of 0.4 g/s and different sample materials at $\alpha = 20°$

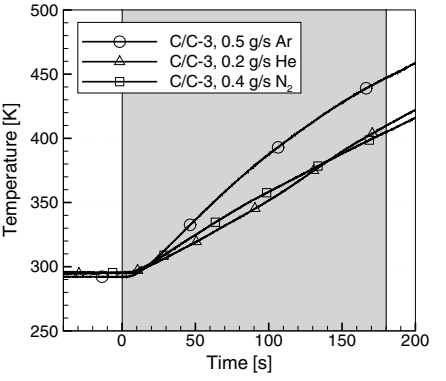

Fig. 18. Under surface temperatures of standard C/C ⊥ for ideal coolant mass flows at $\alpha = 20°$

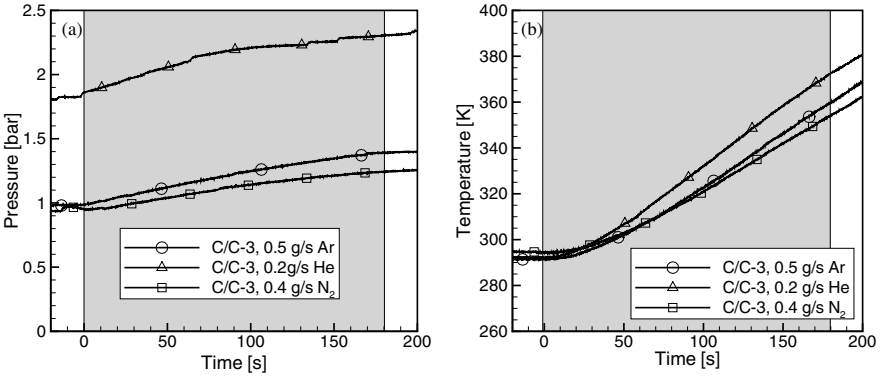

Fig. 19. (a) Reservoir pressures and (b) coolant gas temperatures for ideal coolant gases and standard C/C ⊥, $\alpha = 20°$

Based on the experiences made at $\alpha = 20°$, N_2 mass flows of 0.4 g/s turned out be effective enough at this angle of attack. Therefore, sample materials standard C/C ⊥ and ∥ as well as highly porous C/C have been tested at this mass flow rate, see Fig. 17. The temperature history for both standard C/C materials looks very similar; whereas for highly porous C/C the temperature increases more at the beginning, but turns later to rise with a similar gradient as the other materials.

Adapted from ideal nitrogen mass flows of 0.4 g/s at $\alpha = 20°$, several tests have been conducted in order to find out, which equivalent mass flows are demanded for coolant gases Ar and He. In doing so, Ar mass flows of 0.5 g/s and He mass flows of 0.2 g/s have been detected, which gain similar satisfying cooling effects. Figure 18 shows the under surface temperatures for standard C/C ⊥ and the different coolant mass flows mentioned.

Concerning the application of such a cooling technique, it is also important to know the operating pressures and temperatures of the coolant gases. Figure 19a shows the coolant gas pressures in the reservoir corresponding to the minimal, ideal coolant mass flows mentioned before. The corresponding coolant pressures tend to rise at the tests, because the setup will be heated up from top and so the coolant gas, which can be seen in Fig. 19b.

For He, pressures of about 2.3 bars, while for N_2 and Ar, pressures of about 1.2 – 1.4 bars are reached. It is also remarked, that helium demands approximately 3.5 times higher volume flows than nitrogen for the mass flows compared to achieve similar cooling effects.

Coolant gas temperatures of Ar and N_2 in quite good agreement, He gas temperatures tend to be slightly higher than the others. Ideally, the gas temperatures should be constant, which cannot be avoided at this kind of hot structures due to internal heating. On the other side, high coolant gas flows could eliminate this problem, but this is not desired as the weight for a real spacecraft will be increased and the boundary layer will be disturbed more.

Just as for the screening tests, a comparability number *Z* (which characterises the temperature reduction on the sample under surface) was determined by Eq. 1. Figures 20a and b show the values for *Z* dependent on coolant mass flows for standard C/C ⊥ at $\alpha = 20°$ and 30°. For both angles of attack, the efficiencies are nearly the same, although higher heat loads were applied for $\alpha = 30°$. It can also be seen, that for each coolant gas the efficiency stagnates at a certain point. These points out, that for technical aspects smaller amounts of coolant mass flow are sufficient.

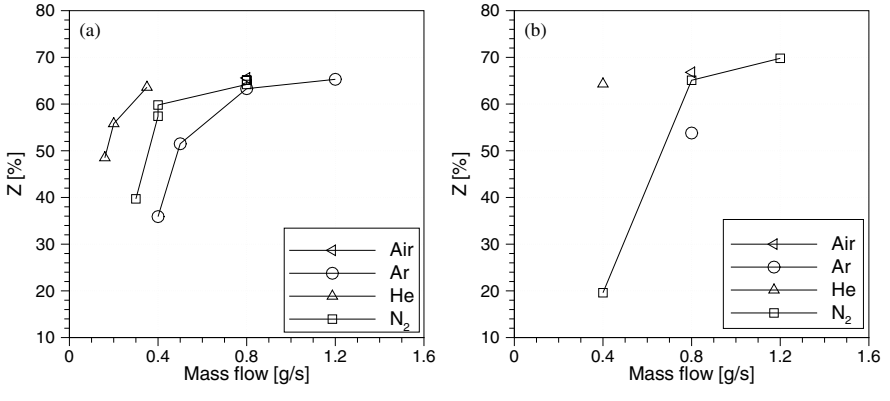

Fig. 20. Comparability number Z for C/C standard ⊥ and different coolant gases, (a) $\alpha = 20°$, (b) $\alpha = 30°$

He seems to be very sufficient compared by mass flows, but compared by volume flows, helium demands much higher volume flows than nitrogen to achieve equivalent cooling. N_2 and air are nearly equal, which was expected due to similar physical properties. Ar turned out to be less effective at same volume flows as already been observed at the screening tests.

Altogether compared at same mass flows, He is most efficient, followed by N_2 and air and Ar at the end. For *Z*, maximum values of 64% for helium, 65% for argon, 67% for air and 70% for nitrogen are achieved.

Figure 21 illustrates the comparability number Z for nitrogen mass flows of 0.4 g/s at an angle of attack of 20°. Contrary to the screening tests, the values for highly porous C/C are slightly lower than for standard C/C. Thereby, the *Z* values of C/C standard ‖ and C/C highly porous correspond to maximum temperatures measured for C/C standard ⊥ material.

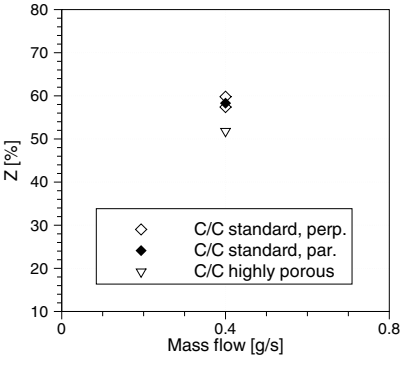

Fig. 21. Comparability number Z for nitrogen mass flows of 0.4 g/s and different sample materials at $\alpha = 20°$

4 Summary

Screening tests conducted in the L2K facility showed, that transpiration cooling at the conditions tested is working well. Sample materials used included C/C standard, C/C highly porous, C/C-SiC and WHIPOX and were tested for coolant gases air, argon, helium and nitrogen. For C/C-SiC and WHIPOX, a higher decrease in under surface temperature was observed, whereat C/C-SiC was based on stratified material and WHIPOX samples were only half as thick as all others. The most homogeneous blowing properties were observed for standard C/C. In total, maximum under surface temperature reductions, characterised by *Z*, of 34% for helium, 36% for argon, 38% for air and 42% for nitrogen were achieved.

Afterwards, a second screening test series in L3K was performed to verify the cooling setup at application relevant conditions. It turned out, that the setup used was not qualified for the more severe flow conditions here. Major sealing problems have been detected, which were very valuable for further investigations.

A new model had been designed and successfully tested in L3K at an even more severe flow condition and two angles of attack (20/30°). Leakage flows of about 3-4‰ were determined, which can be neglected. Three materials, standard C/C with coolant flows parallel and perpendicular to the material's fibre layers and highly porous C/C, were tested. Coolant gases used were air, argon, helium and nitrogen. Although the sample exit area was enlarged by 32%, the appropriate coolant mass flows detected to achieve satisfying cooling effects were much lower compared to the

screening tests. Thereby, minimal ideal coolant mass flows of 0.5 g/s Ar, 0.2 g/s He and 0.4 g/s N_2 were determined; for this mass flows, Z values were between 50-60%. Altogether, under surface temperature reductions Z of 64% for helium, 65% for argon, 67% for air and 70% for nitrogen were achieved.

These test series verified that transpiration cooling can be applied successfully for hot structures at application relevant re-entry conditions. For all tests performed, no significant disturbances of the flow fields have been observed.

To compare the cooling efficiency more precisely, investigations of e.g. effective sample pore exit area, incoming heat fluxes onto the sample and free stream conditions at the sample position have to be done. This would enable the determination of cooling efficiency $\eta(F)$, which is commonly used in the literature.

References

1. Belletre, J., Bataille, F., Lallemand, A.: A New Approach for the Study of Turbulent Boundary Layers with Blowing. International Journal of Heat and Mass Transfer 42, 2905–2920 (1999)
2. Ghadiani, S.R.: A Multiphasic Continuum Mechanical Model for Design Investigations of an Effusion-Cooled Rocket Thrust Chamber. Ph.D. thesis, Universität Stuttgart, Germany (2005)
3. Glass, D.E., Dilley, A.D., Kelly, H.N.: Numerical Analysis of Convection / Transpiration Cooling. Journal of Spacecraft and Rockets 38, 15–20 (2001)
4. Gülhan, A., Esser, B.: Arc-Heated Facilities as a Tool to Study Aerothermodynamic Problems of Reentry Vehicles. In: Lu, F.K., Marren, D.E. (eds.) Advanced Hypersonic Test Facilities, Progress in Astronautics and Aeronautics, vol. 198, pp. 375–403. AIAA (2002)
5. Gülhan, A., Esser, B., Koch, U.: Experimental Investigation on Local Aerothermodynamic Problems of Re-entry Vehicles in the Arc Heated Facility LBK. Journal of Spacecrafts and Rockets 38, 199–206 (2001)
6. Heidenreich, B.: Herstellung von Faserkeramiken nach dem Flüssigsilicierverfahren (LSI-Technik). In: Krenkel, W. (ed.) Keramische Verbundwerkstoffe, pp. 48–75. Wiley-VHH, Weinheim (2003)
7. Heidenreich, B., et al.: Net Shape Manufacturing of Fabric Reinforced Oxide/Oxide Components via Resin Transfer Moulding and Pyrolysis. In: Proceedings of 28th International Cocoa Beach Conference and Exposition on Advanced Ceramics & Composites, Cocoa Beach, USA, January 25-30 (2004)
8. Hwang, C.B., Lin, C.A.: Low-Reynolds number k-epsilon Modelling of Flows with Transpiration. International Journal for Numerical Methods in Fluids 32, 495–514 (2000)
9. Kays, W.M.: Heat Transfer to the Transpired Turbulent Boundary Layer. International Journal of Heat and Mass Transfer 15, 1023–1044 (1972)
10. Kuhn, M., et al.: Experimental Investigations of Transpiration Cooled CMC's in Supersonic Plasma Flows. In: Proceedings of 5th European Workshop on Thermal Protection Systems and Hot Structures, Nordwijk, Netherlands, ESA SP-631 (2006)
11. Lezuo, M.K.: Wärmetransport in H2-transpirativ gekühlten Brennkammerkomponenten. Ph.D. thesis, RWTH Aachen, Germany (1998)
12. Luikov, A.V.: Heat and Mass Transfer with Transpired Cooling. International Journal of Heat and Mass Transfer 6, 559–570 (1963)
13. Rannie, W.D.: A Simplified Theory of Porous Wall Cooling, JPL California Institute of Technology, Pasadena, USA (1947)

14. Rodet, J.C., et al.: Etude en souflerie thermique du refroidissement de parois poreuses par effusion de gaz. Revue Generale de Thermique 37, 123–136 (1997)
15. Rubesin, M.W.: An Analytical Estimation of the Effect of Transpiration Cooling on the Heat-Transfer and Skin-Friction Characteristics of a Compressible, Turbulent Boundary Layer. NACA TN 3341 (1954)
16. Rubesin, M.W., Pappas, C.C.: An Analysis of the Turbulent Boundary-Layer Characteristics on a Flat Plate with Distributed Light-Gas Injection. NACA TN 4149 (1958)
17. Schmücker, M., Grafmüller, A., Schneider, H.: Mesostructure of WHIPOX all Oxide CMCs. Composites, Part A 34, 613–622 (2003)
18. Serbest, E.: Untersuchungen zur Anwendung der Effusionskühlung bei Raketenbrennkammern. Ph.D. thesis, RWTH Aachen, Germany (2002)
19. Sucec, J., Oljaca, M.: Calculation of Turbulent Boundary Layers with Transpiration and Pressure Gradient Effects. International Journal of Heat and Mass Transfer 38, 2855–2862 (1995)